NB SPUTTER COATING ON QWR IN ANU

N.R. Lobanov and D. C. Weisser

Nuclear Physics Department, Research School of
Physical Sciences and Engineering,
Australian National University, ACT, Canberra 0200, Australia

ABSTRACT

Nb sputtered QWRs are to be used for the future extension of the Linac. The magnetron sputtering system and its operational performance are described. A magnetron discharge in argon is used for sputtering niobium and in helium for cleaning of the resonator. The cathode comprises two cylindrical and one ring element. The I-V characteristics of the sputtering in argon are given. The superconducting film is deposited with a uniform film thickness and coverage of the resonator. The distribution of the deposition rate from different cathode-resonator geometry and film thickness profiles are discussed. The switching of the cylindrical sputtering cathode from external to internal regions of the cathode, is described. A sputtering procedure, test depositions on ceramic samples and sputtering on the QWR for Time-Energy Lens, will be outlined. The composition of impurities stemming from the sputtering process, will be discussed.

1. Introduction

The ANU accelerator system, comprising the 14UD and Linac, continues to evolve toward a competent integrated research facility. The Linac successfully passed important milestones in 1996, including the first nuclear physics experiment performed on 5 June, and its official inauguration on 11 July.

Good progress has been made in the conditioning of the Pb plated, split loop resonators. Combinations of pulsed RF power conditioning and helium conditioning have enabled all resonators to operate near and above 2 MV/m.

This has encouraged the continued short term use of these resonators without replating and provides the opportunity for the exploitation of more modern lead plating technology, in the next two years.

The focus of this report is, however, on Nb sputter coating technology. Improvements to the Nb sputtering apparatus and procedures will be exploited in the production of the quarter wave resonator to be used in the Time-Energy Lens which time focuses the beam or homogenizes its energy.

For the future extension of the Linac, Nb sputtered QWRs are to be used. The sputter-coating technology produces cavities with very good RF performance at electric field below 5-7 MV/m. However, as the field increases, the RF quality factor, Q, of the niobium-coated cavities quickly reduces. Research at CERN suggested that the main cause of Q degradation is the effect of impurities in the Nb film [1].

This paper, in Section 2, describes the mechanism of surface contamination accompanying the preparation of bulk copper QWRs for coating (mechanical polishing and cleaning, chemical etching and cleaning). Because the RF field only penetrates about 50 nm, the surface region of the niobium film is crucial. If the surface region is high in impurities, then the transition temperature might be lower and thereby give higher losses. Also, regions with high oxygen concentration might be sites of thermal breakdown. In any case, it should be noted that the surface is the key to understanding RF superconductivity. Based on theoretical investigations of Ref. [2,3], we pursue the hypothesis that the source of the oxygen problem is the protective oxide layers on system surfaces exposed to various discharge constituents: electrons, ions and ultraviolet photons. The bombardment by them stimulates decomposition of the surface oxide and desorption of oxygen and other surface contaminants into the residual atmosphere. Of particular importance is the control of the copper surfaces prior to sputter coating.

In Section 3, a design of the sputtering system and its operational performance are described. Magnetron discharges from a two cylindrical and one ring cathode, in argon and in helium, were used for sputtering niobium and for cleaning of the resonator. The I-V characteristics of sputtering system in argon are given. The sputter coating system operates at 360-380V

discharge voltage at 2-5 mTorr argon pressure. Extremely efficient confinement and directional control of electrons ("balancing") results in excellent target utilization, low pressure operation and a broad stable plasma discharge across the cathode surface.

The superconducting film should be uniform in thickness over structures like the shaped end electrode, beam holes, coupler and sniffer holes. The distribution of deposition rate from the complex cathode-resonator geometry and film thickness profiles are discussed in Section 4.

The resonator surface in contact with the plasma is bombarded with electrons, ions, energetic neutrals and photons all of which can have serious effects during film growth. It has been demonstrated that low-energy ion irradiation has an important role in controlling nucleation and growth kinetics of film. In Section 5, we summarize some results on magnetron sputtering combined with biasing the resonator. Substrate bias has an important influence on the quality of the deposited films and process yields. Some preliminary results on magnetron bias sputtering are also discussed.

In Section 5, the control of switching the discharge from external to internal area of the cylinder sputtering cathode is described for the old cathode. The ignition potential of the outer gap was smaller than that of the inner gap and so the discharge ordinarily exists in the outer gap only. A small magnetic field from the external solenoid or alternatively, resonator bias, are used to create additional leakage from the electron trap in the outer gap, increasing its ignition potential. Switching this solenoid or resonator bias controls on which side of the cylindrical cathode the discharge occurs.

In Section 6, a sputtering procedure, test depositions on ceramic samples and sputtering on a QWR for the Time-Energy Lens, are described. The concentration of impurities in Nb can be assessed by the measurement of the residual resistivity ratio [3,4] $RRR = 1+3.2\alpha^{-1}$, where α is the concentration of oxygen, nitrogen or carbon in niobium, at.%. Due to its high chemical affinity to niobium, oxygen is the most deleterious.

The RRR value alone does not specify the nature of impurities. The composition of impurities stemming from the sputtering process, will be

discussed. A brief discussion of RF cavity problems and how non-ideal surfaces affect these devices is given.

2. Preparing of bulk copper QWR for coating

Niobium performs as an excellent getter during its sputtering onto a copper substrate. For instance, the Nb-O binding energy is higher than that of Nb-Nb. For that reason, the quality of Nb film deposited onto copper a QWR depends crucially on the conditions on the copper substrate which supplies oxygen to the discharge. The sequence of mechanical and chemical polishing of the copper substrate consists of the following main steps: 1) mechanical polishing (hand and tumbling); 2) ethanol rinsing, low pressure and high pressure ultrapure water rinsing (LPR and HPR); 3) RBS35 detergent treatment; 4) chemical polishing; 5) surface passivation; 6) high pressure ultrapure water rinsing; 7) high vacuum baking. The first step is carried out in normal atmosphere. The steps 2-6 occur in a filtered air pressurized room.

The final surface finishing for lead plating SLR was varied in [5]. Surprisingly Ref.5 reports that the 'dirty' resonators hand-lapped with 2 micron non-embedding garnet compound conditioned far more readily than 'clean' CERN-polished ones and all resonators achieved $Q \geq 10^8$ at 3 MV/m.

2.1 Mechanical Polishing

2.1.a Shorting plate- hand polishing

Because of very the complicated shape of the QWR and non-uniform tumbling on the shorting plate, the mechanical polishing of the shorting plate is done by hand in three steps. Tin oxide is applied with special tools on the flat shorting plate surface and on the transition radii from it to the resonator wall and to the central stub (Figure 1).

The polishing device consists of a tubular driving shaft that can be equipped

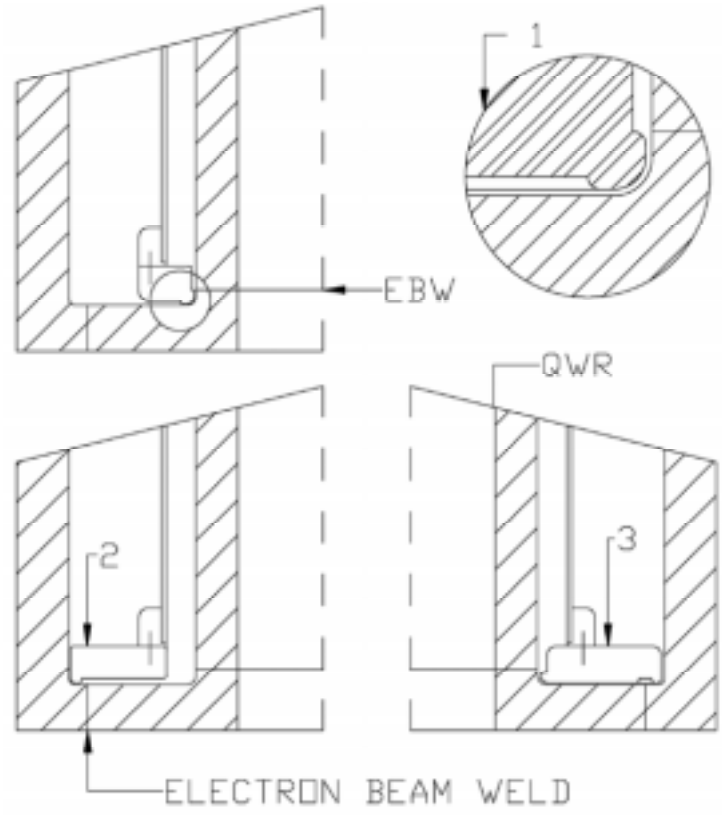

Figure 1 Device for hand polishing on shorting plate:
1- inner radius; 2- outer radius; 3- flat surface.

with the three different tips. Particular care has been taken in tip design in order to avoid the electron-beam welds. With the resonator in a vertical position (shorting plate down), ~ 50 ml of abrasive mix tin oxide with deionized water is poured in. Up to twelve 1 cm wide and ~.3 mm thick DURX 670 cloth strips are fitted radially onto the tip providing effective carriers and applicators of abrasive to the shorting plate surface. Up to thirty minutes of polishing with the device was required.

2.1.b Tumbling

The resonator was then tumbled with ANU designed mixes for 2 to 3 days in four steps decreasing the size of the abrasive media from 800 to 1200 grit (3 μm). The surface morphology, as observed by SEM on copper samples after different tumbling stages, is shown on Figure 2 (a,b).

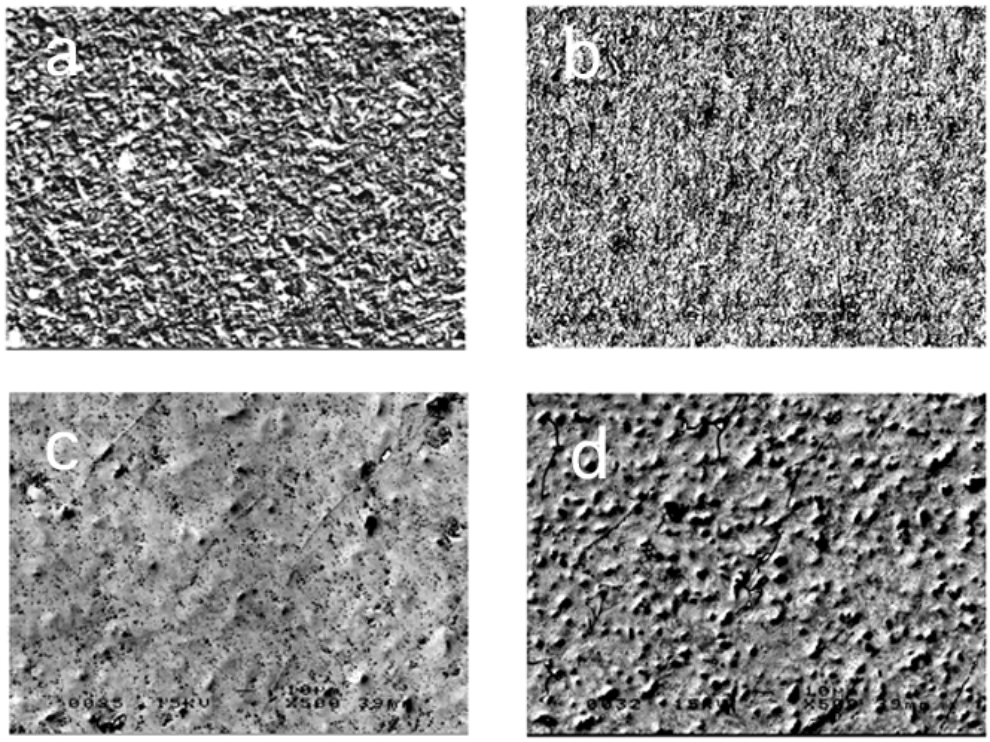

Figure 2 The surface morphology of copper samples observed by SEM: a- tumbling 60 μm abrasive; b- tumbling 1 μm abrasive; c- chemical polishing removing 10 μm; d- chemical polishing removing 30 μm.

An elemental surface analysis carried out by X-ray emission shows the presence of the carbon, aluminium and silicon on the copper surface. This contamination of tumbling components is removed effectively during HPR. All stages of tumbling require that the resonator body is approximately half full of mixture when it is laying level on its side (~6 liters). The mixture should be observed to "tumble", that is, that it will rotate in the body and fall down the slope formed diagonally across the middle. It is essential to thoroughly wash out the resonator between each stage of tumbling and to keep all mixtures in sealed containers to avoid contamination. The ANU tumbling recipes are given in Table 1. The length of the procedure depends on the starting condition of the surface. The surface roughness after final tumbling was estimated as R_a=0.25 micron (Figure 2b). Mechanically polished copper surfaces give highly-uniform fine-grained appearance free of bulk imperfections such as porosity, loosely adhering flakes, etc. These may

release chemicals under vacuum or compromise both adhesion of the Nb film and so its thermal anchoring.

2.3 Rinsing

Degrease and clean copper after tumbling for 30 minutes in 2% RBS35 or Decon90 at 50 C° followed by rinsing in ethanol and three high pressure rinse (HPR) in deionized water.[1]

2.4 Chemical Polishing

The chemical polishing recipe is based on CERN polishing bath [6]. The bath works satisfactory only at 70±2 C°. The bath must be vigorously agitated for 5-6 minutes to achieve ~7-9 μm etch. The surface finish after chemical removal of surface layers of different thickness is shown in Figure 2(c,d).

Table 1.
ANU recipes of the tumbling mixes for four different steps

N	Mix Composition	Abrasive, μm	Time, Hrs	Rate, μm/day
1	*Rough Grinding*: plastic cones 0.5" diam, 5.5 l; FAC200 (wetting agent), 2.5 kg; DW*	-	72	20.0
2	*Susan*: PP, 1.5 kg; AO, 1.2 kg; R50, tbs; DW	800 grit, 4 μm	48	4.1
3	*Allan*: PP, 4 kg; AO, 2 kg; GB, 2.5 kg; R50, tbs; DW	1200 grit 3 μm	48	0.45
4	*George*: PP, 4 kg; TO, 1 kg; GB, 2.5 kg; DW, 1.2 l; alhogol (wetting agent)	1200 grit 3 μm	48	0.25

*)DW- de-ionized water; PP-plastic pellets 0.25"x0.25"; AO- aluminium oxide; tbs- table spoon; GB- glass beads, 0.125" diam.; TO-tin oxide.

[1] RBS35 is a comercial detergent manufactured by CHEMICAL-PRODUCTS, Belgium. Composition: anionic and non-ionic surfacting agents, phosphates and polyphosphates, hydrates and chlorinated agents.[1]

Surface pitting is generally observed on all samples which tends to increase with etching time. Samples were made of bulk OFHC copper. Pronounced pitting for large surface thickness removal of up to 30 μm (Figure 2d) is the result of the creation of hydrogen bubbles sticking to the sample surface which cannot be removed by agitation. Therefore it has been decided to chemical polish the QWR for 5-6 minutes only making a compromise between the cleanness and roughness of the copper surface. No sign of chemical/tumbling contamination was found by SEM technique after etch though this technique might miss thin surface stains.

2.5 Surface Passivation

5 gm/liter citric acid is applied as passivation solution followed by three HPR with deionized water aiming to produce copper surface with thinnest possible oxide layer in order to minimize the inventory of oxygen available to contaminate the Nb.

2.6 Ultrapure Water Rinsing

High pressure water rinsing is done by feeding ultra clean (resistance at room temperature higher than 8 Mohm cm) water to high pressure pump which produces ~6 l/min of water at 50 bar. The spray nozzle is made of 304 stainless steel. Prior to the application of the HPR, the pump is operated for a few minutes in order to purge it of possible contamination. The resonator is rinsed for ~10 min after each chemical step. The rinsing system is far from being optimized. Nevertheless, HPR can improve surface cleanliness resulting in improvements in Q-value and field emission behavior [7]. HPR is followed by drying in dry nitrogen gas. We excluded alcohol drying from the procedure because it left too many stains. A suitable protective atmosphere (continues dry nitrogen flow) is of considerable importance in reducing absorbtion of oxygen by remaining water drops and thus in preventing strong copper oxidation. The type of oxide that can be formed depends on the proportion of oxygen in the drying atmosphere and the actual temperature. The temperature also determines the reaction rate and, hence, the thickness of the oxide film.

The rate of oxidation depends largely on the thickness of the moisture layer on the metal surface [8]. With a very thin (10-100nm) moisture film, the rate of oxidation is not much different from that of dry oxidation, that is, the oxidation action has a purely chemical character. With increased

thickness (about 10 μm) the rate of oxidation starts to increase rapidly because the film begins to act as an electrolyte and the oxidation action becomes electrochemical in character. The rate of oxidation reaches a maximum and then decreases with further increase in film thickness when a visible moisture layer is present on the surface, this is a range of wet atmospheric oxidation. In atmospheric oxidation, the outstanding promoting factors are associated with the presence in the atmosphere of low concentrations of H_2S and SO_2. The film thickens approximately follows a parabolic form, $W^2 = kt$, where W is the thickness of the film, t is the time and k is a constant. At room temperature, the oxide layer reaches a maximum thickness of 2-3 nm in one hour in dry protective atmosphere. The pressure-temperature stability region for Cu_2O and CuO (10^{-4}-10^4 Torr and 0-1000° C) is given in [9]. At atmospheric pressure and room temperature, the oxide film should be wholly Cu_2O.

2.7 High Vacuum Baking

The final operation before sputtering is high vacuum baking at 170°C at 10^{-6} Torr pressure for 140 hours. Baking promotes desorbtion of water vapor which contains unwanted oxygen.

3. Design and operational performance of the sputtering system

The apparatus shown schematically in Figure 3 consists of an assembly of the three magnetron cathodes inserted inside the resonator. Each cathode includes a ring of Alnico 5 permanent magnets, water-cooling system, niobium cladding (0.5 mm thick Nb sheet, RRR = 142), and shielded ceramic insulators. The copper water-cooling base, 6.35 mm diameter stainless steel tubes and auxiliary support structure, usually operate at floating potential. When the support structure is connected to the cathode, it draws up to 0.2% of the discharge current in the case of the cylindrical cathodes, and up to 0.7% for ring cathode. Therefore, to avoid contamination due to cathode sputtering from non Nb surfaces, all surfaces of the support structures and insulator shielding connected to the cathode, were covered with Nb sheet of RRR = 13. To provide uniform film thickness along the resonator, the cathode assembly is scanned along the axis. During the scan, the geometry of resonator to cathode varies significantly, however the discharge voltage

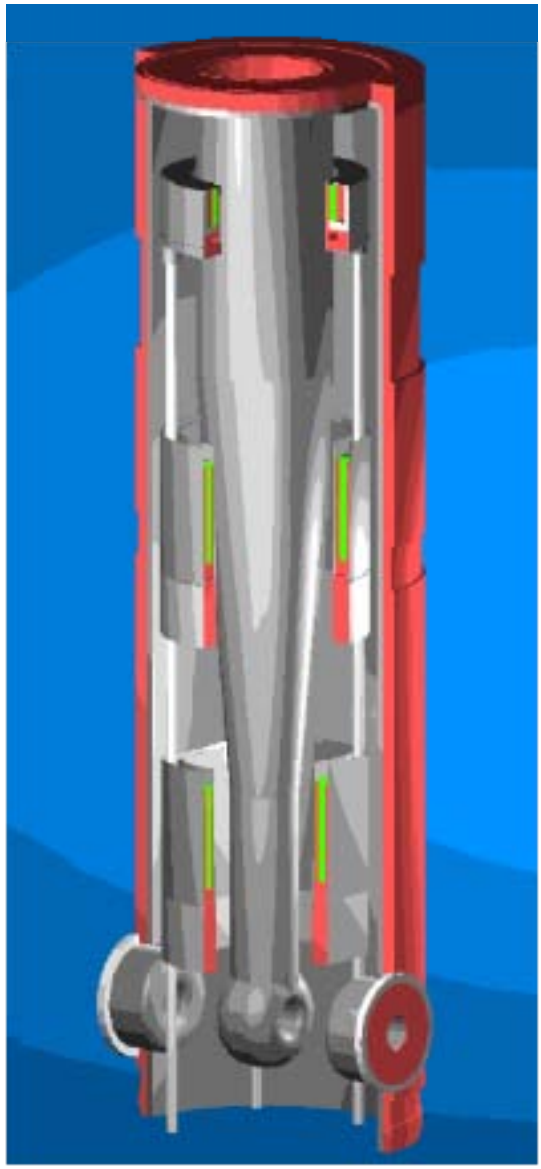

Figure 3 Quarter-wave resonator with magnetron sputtering assembly. At the top is the ring cathode, in the middle and bottom are the cylindrical cathodes.

stays constant within ± 1%. During sputtering, beam holes and the coupler hole are covered externally with copper strip to prevent parasitic discharge escaping into the vacuum vessel.

Copper and ceramic samples are installed below the resonator for further RRR and surface structure analysis after deposition. The system is pumped by a 150 l/s turbo-molecular pump, an 60 l/s ion pump (isolated during

coating) and 2000 l/s titanium sublimer pump. The base pressure is $5x10^{-9}$ Torr after bakeout for 180 hours at 280-300 °C.

Although grade 5, 99.999% ultra high purity argon or helium are used during sputtering and cleaning, the feed gases may still contain up to 10 ppm of oxygen, nitrogen and water. The gas feed plumbing uses stainless steel and just before entering the discharge space, the ultra pure gas is passed through the titanium sublimer pump. Our estimation is, that before ignition of the discharge at typical 3 mTorr, the partial pressure of the oxygen-containing gases in the residual atmosphere does not exceed $3x10^{-9}$ Torr.

In magnetron sputtering, a magnetic field is used to trap electrons near the cathode, allowing operation at low argon pressure. The cylindrical cathodes 1 and 2 employ magnetic circuits producing axial magnetic fields alongside the cylindrical emitting surfaces which terminating back near the cathode ends. The magnetic field first used in the ring cathode had two shortcomings. Firstly, the sputtering was so localized, that the Nb sheet was quickly worn through. Secondly, the field was so low (170 Gauss at 5 mm above Nb cladding), that the cathode needed to operate at an undesirable high argon pressure, 50 mTorr. A new cathode was designed using the Superfish code to optimize the magnetic field increasing it to 250 Gauss. The magnetic field distribution adopted for the ring cathode as well as the magnetic field of the cylindrical cathodes is shown in Figure 4. Extremely efficient confinement and directional control of electrons ("balancing") results in excellent target utilization, low mTorr operation and a broad stable plasma discharge across the target surface. These features have important influences on the quality of the deposited film and process yields.

Discharges operating in the magnetron mode obey an I-V relationship of the form $I \sim V^n$, where n is an index of the performance of the electron trap and is typically in the range 5 to 9 [12]. Experiments by Rossnegel [13] measured an apparent pressure reduction in the region near the magnetron cathode, due to heating of the gas by the plasma and the sputtering process. The energy of sputtered particles is usually in the order of 10 eV and the thermallization process of these sputtered atoms can cause a considerable reduction in the gas pressure in front of the sputtering source. For example, ref.11 reports that when the probe was located 5.3 cm from the cathode surface in 7.5 mTorr Ar pressure at 15 mA/cm^2 magnetron current density, the measured

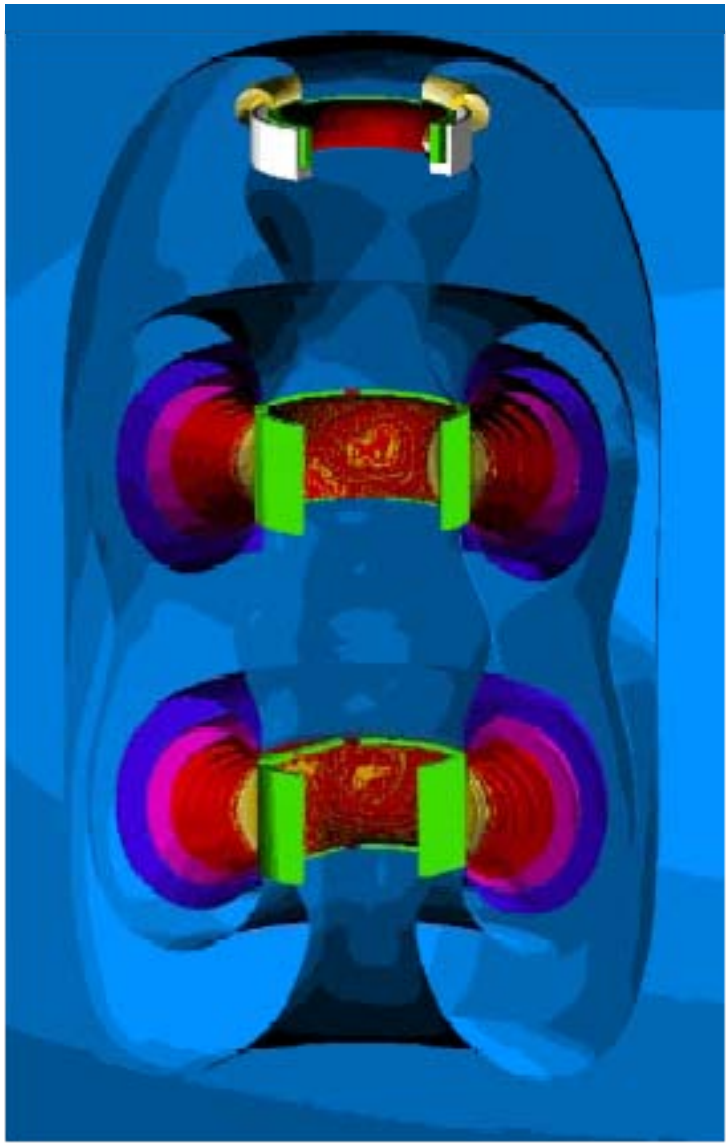

Figure 4 Calculated magnetic field distribution in the ANU magnetron cathode assembly.

pressure reduction can be as much as 85%. This effect should be present for the ANU magnetron which has a similar configuration and operation parameters. The magnitude of the density reduction observed in front of a magnetron cathode suggests that this will be an important feature in the understanding of both the physical processes in the magnetron plasma as well as the effect on the depositing films. At high magnetron discharge currents, the reduction in gas density will tend to drive the plasma impedance up, resulting in higher voltage and higher sputter rates both of which reduce the oxygen poisoning effect on the Nb film during sputtering.

Typical I-V curves for ANU magnetron assembly operating with various discharge orientations and pressures are shown in Figures 5 and 6.

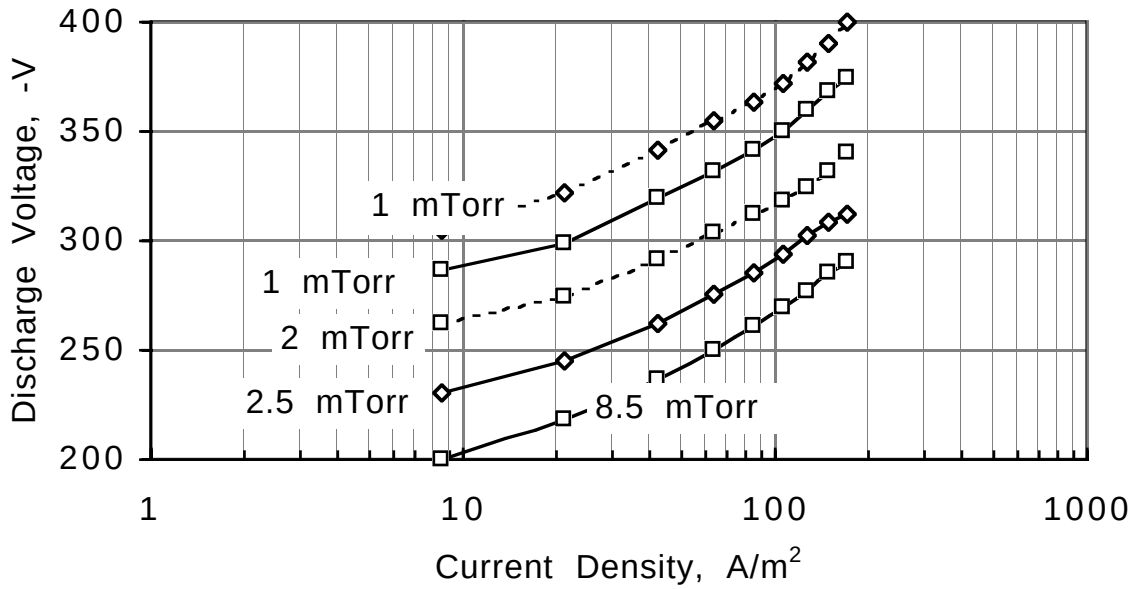

Figure 5 Typical current-voltage characteristics for cylindrical magnetron cathode (magnetic field of 200 G, 5 mm above the target). No external magnetic field. Solid line: resonator grounded; dashed line: resonator insulated.

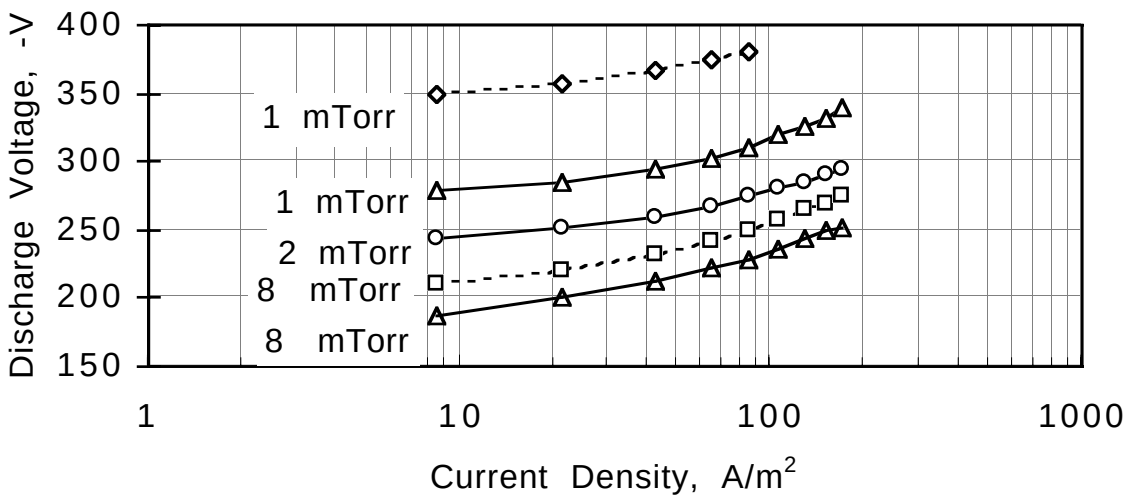

Figure 6 Current-voltage characteristics for ring cathode (magnetic field of 250 G, 5 mm above the target), solid line: resonator grounded; dashed line: resonator insulated.

When the resonator is grounded, the cylindrical cathode is a cylindrical-post magnetron (discharge in the outer gap) and a cylindrical-hollow magnetron (discharge in the inner gap) [11,12].

The rate of the sputtering of the cathode is determined by mechanical measurement of its profile with TESATAST probe with accuracy of 0.01 mm. The sputtering of the cylindrical and ring cathodes is not uniform along the whole of their active surfaces. As is seen from Figure 7, the normalized sputtering rate is greatest at the center of each structure. Because of the

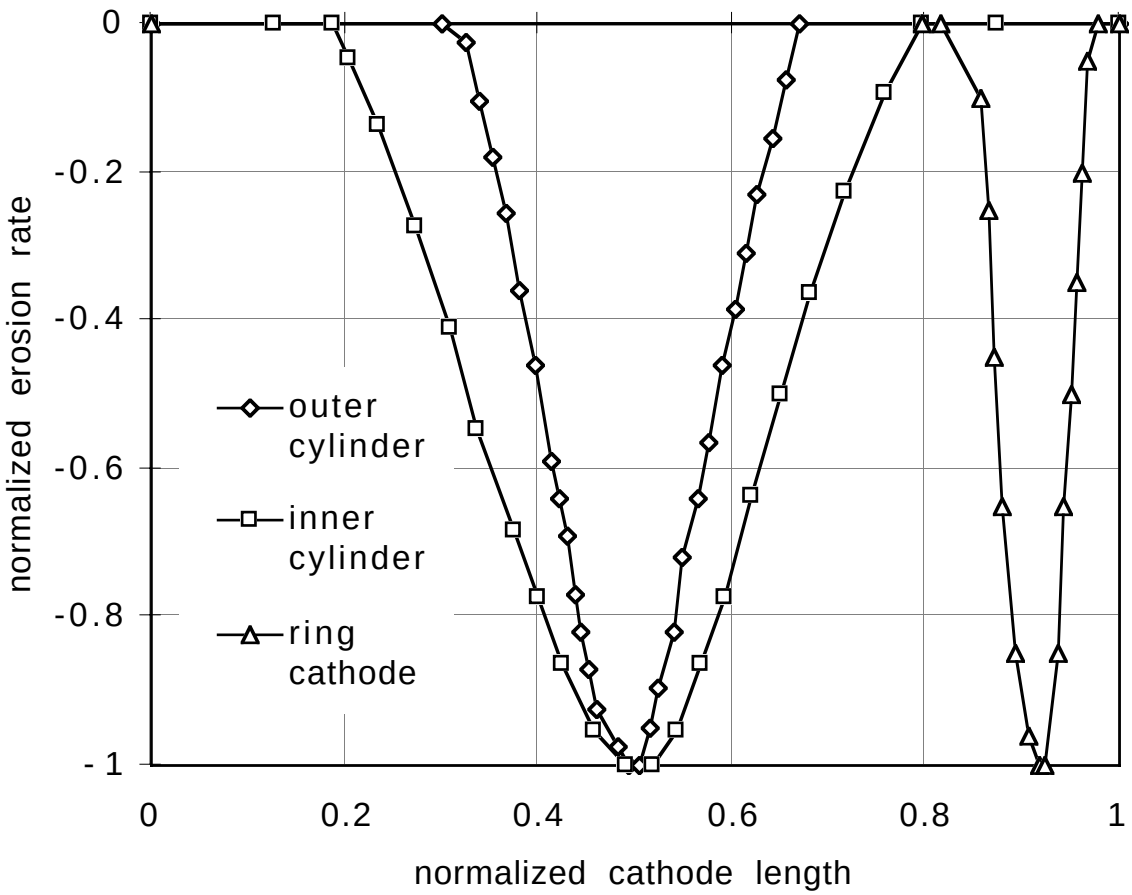

Figure 7 Normalized sputtering rate distribution from cylindrical and ring cathodes. Zero radius for the ring cathode corresponds to the axis of symmetry.

greater length of the cylindrical cathodes, this nonuniformity is less pronounced. On the inner side of the cylindrical cathode, the sputtering length is greater than on the outer side, approximately 60% of the cathode length. Since the ring cathode has a complex form, one naturally expects a

different degree of sputtering of its separate parts. Although sputtering also occurs on its vertical surfaces, it is an order of magnitude weaker than on the top face.

4. Niobium deposition rate

The superconducting film, should be uniform in thickness over structures like the shaped end electrodes, beam holes, coupler and sniffer holes. The distribution of deposition rate from different cathode-resonator geometry and film thickness profiles is discussed.

4.1 Critical Nb Deposition Rate.

In establishing a procedure for a coating process using a sputter-deposition technique, it is important to find a range of sputtering-gas pressures to give appropriate film properties in a given. One of the main ways through which the sputtering-gas pressure affects film properties is oxygen poisoning when Nb atoms interact with absorbed oxygen-containing molecules on the substrate surface. The oxygen diminishes the transition temperature of the pure Nb from 9.2 K by 1 K per each atomic percent [14]. The partial pressure of the oxygen-containing gas may be estimated by [15]:

$$P_O \cong 1.3x10^{-9}\alpha\delta\sqrt{T}\exp(0.00625T), \quad \text{Torr}, \quad (1)$$

where α is the oxygen concentration in the Nb film, at.%; δ the Nb deposition rate, μm/h; T the substrate temperature, K. If the goal oxygen contaminant is taken to be α = 0.01% (RRR=330) one can calculate a critical Nb deposition rate of δ_{crit} = 1.5 μm/h assuming, $P_{crit} \cong 3x10^{-9}$ Torr, T = 300 K. This does not take into account the pressure reduction due to sputter current. The sputtering procedure and discharge parameters have to be optimized so that the actual deposition rate exceeds the critical rate over the whole surface of resonator. This has led to the use of only one active cathode at a time in order to concentrate the available current so that the critical rate of 1.5 μm/h is exceeded.

The second important effect of gas pressure is scattering of sputtered particles during their flight from the target to a substrate. In cases where sputtered particles travel a much longer distance than their mean free path, the gas scattering becomes important. The mean free path between

collisions of gas molecules or atoms is most simply calculated treating them as hard spheres in which the collision cross section is related to the diameter of the spheres [19]. In sputter deposition, the mean free path of sputtered Nb atoms with mass M_{Nb} which are traveling through Ar gas with mass M_{Ar}

$$\lambda^{-1}=\sqrt{2}N_{Nb}D_{Nb}^{2}+0.25\pi\, N_{Ar}(D_{Nb}+D_{Ar})^{2}(1+M_{Nb}/M_{Ar})^{0.5} \quad (2)$$

where N_{Nb} and N_{Ar} are the density of sputtered atoms and Ar gas, D_{Nb} and D_{Ar} are the diameters of the particles. T. Motohiro applied Monte Carlo simulation including gas scattering in the analysis of a sputter-deposition process [16]. Westwood [17] has calculated the average energy retained by an atom of mass M_s in collisions with a atom of mass M_g as well as the average angle of deviation due to the collision. Nb atoms traveling through Ar gas, would lose 30% of their energy and be deflected 10° in each collision. Somekh in [18] presented a calculation of the rate of energy loss of sputtered atoms and reflected neutrals due to elastic collisions with the sputtering gas atoms with a temperature of 500 K. The average initial energy of the sputtered atoms is 10-30 eV. The typical pressure distance product for sputtered Nb atoms, with initial energies of 20-30 eV, to lose 90% of their energy ($PD_{0.1}$) is 10-12 mTorr cm in Ar. The sputtered and reflected neutral atoms arriving at the substrate will have a finite energy and associated momentum. Because of the transfer of momentum in the collision process, Ar gas atoms, which collide with these sputtered and reflected neutral energetic atoms, will also bombard the substrate. The effect of these collisions is to establish a dynamic equilibrium through transfer of energy to the sputtering gas and the depositing of this energy in the substrate.

The main conclusion is that, for the ANU sputtering system, the thermalization tends to be incomplete because the pressure distance product PD for cylindrical cathodes in Ar is 0.4 - 0.6 mTorr cm and for the ring cathode, in the top stationary position, is 4 mTorr cm. However, when complete thermalization of Nb reaching the shorting plate is likely the ring cathode is at the bottom of the scan used to coat the walls and stub. In order to insure that the plate coating is of adequate quality, this scan ends with the cathode 4.5 cm from the plate.

Finally, based on theoretical investigations of Ref. [2,3], we pursue the hypothesis that oxygen from the copper oxide layer degrades the deposited film.

4.2 Thickness Distribution

The Nb coverage is calculated by integrating contributions from point sources on the cathodes over the total area of the resonator [19]. This is justified because the 5.6 cm mean free path of Nb is comparable to the distances between cathodes and substrate. Thus the flux of ejected particles is assumed to travel without collisions, and to decrease with distance as r^{-2}. Therefore, for a given source geometry, the film thickness distribution can be calculated purely geometrically. Such calculations, assuming a linear errosion distribution for the ANU geometry, were given in [15]. In this paper, simulations were done taking into account the measured erosion of the target-cathode (see Figure 7). The deposition rate $\delta[\mu m/h]$ from the cathode surface onto a small area around point A on a substrate in cylindrical coordinate system is [15]:

$$\delta(l)=5.1x10^{-3}\,KJ(U-90)^{0.58}\iint\rho(l,x,\varphi)^{-2}\cos\alpha(l,x,\varphi)\cos\beta(l,x,\varphi)\,F(x)d\varphi dx \quad (3)$$

where:
K equals b^{-1} for the cylindrical cathode and $r_c b^{-1}$ for the ring cathode;
r_c is the mean radius of the ring cathode, cm;
$J[mA]$ and $U[V]$ are the discharge current and voltage;
$2b$ is the length of the sputtered cathode surface, cm;
ρ is the distance between $d\varphi dx$ and point A, cm;
α is the two-dimensional angle between ρ and the surface element on the substrate around point A, rad;
β is the similar angle between ρ and surface element of the emitting surface $d\varphi dx$;
$F(x)$ is the normalized erosion rate of the cathode fitted with polinominal trendline of 5th-6th order described in section 3;
φ_{max} is the maximum angular coordinate of the point on the emitting surface, visible from the point A.

The parameters of equation (3) for the various cathode-resonator geometries were estimated in [15] with the exception of $F(x)$. A quantitative connection between sputtering rate $\delta(l)$ and discharge current J was

established and calibrated in [20] by direct measurements of film thickness based on the SIMS technique. Geometrical equations describing parameters ρ, $cos\alpha$ and $cos\beta$ are also given in ref.20. Calculations of deposition rates from cylindrical cathodes were made assuming that the Nb electrodes are two concentric cylinders. In reality, the bottom cylindrical cathode has flats resulting in asymmetry of the deposition rate around resonator axis. However, the shape change due to the flats is not large and, for many practical purposes, the cylindrical model can be used. More serious disruptions are introduced by the doughnuts around the beam holes (Figure 3). The complicated shape of the doughnuts makes comprehensive calculations of the deposition rate in this area too cumbersome. Fortunately, the beam holes are in the low magnetic field area of the QWR where the uniformity of the Nb film is not critical. The flattened cylindrical cathode provides an uninterrupted discharge and visually uniform coverage while scanning over the doughnuts area.

4.3 Ring Cathode and Cylindrical Cathode

Figure 8 depicts the deposition rate from the ring cathode for a range of positions, *l*, of its top surface to the shorting plate. The emitting surface is a horizontal ring with mean radius r_c = 5.1 cm and width $2b$ = 1.75 cm. All distribution curves are calculated at J = 1 Amp discharge current and can be used for other discharge current by scaling. The discharge current in the ANU sputtering cathode, up to 3 A, is limited by the magnetron power supply. The deposition rate onto the shorting plate exceeds the critical magnitude of 1.5 μm/h over the its whole area with average rate of 2.8 μm/h, when the ring cathode is stationary l = 4.5 cm below the shorting plate. This coincidentally, matches the Nb mean free path.

The deposition rate from the ring cathode onto inner stub is about four times higher than to the outer wall. This effect on film thickness will be discussed later. Figures 8 and 9 show deposition rates from the ring cathode and cylindrical cathodes, when stationary, onto the outer wall of the resonator and stub. The emitting surface of the cylindrical cathode is a cylinder with radius r_c = 6.0 cm; width $2b$ = 2.4 cm for the outer surface and r_c = 5.2 cm; $2b$ = 4.8 cm for the inner surface. Deposition onto the stub was calculated for different parts of the stub using the radii at the top of the

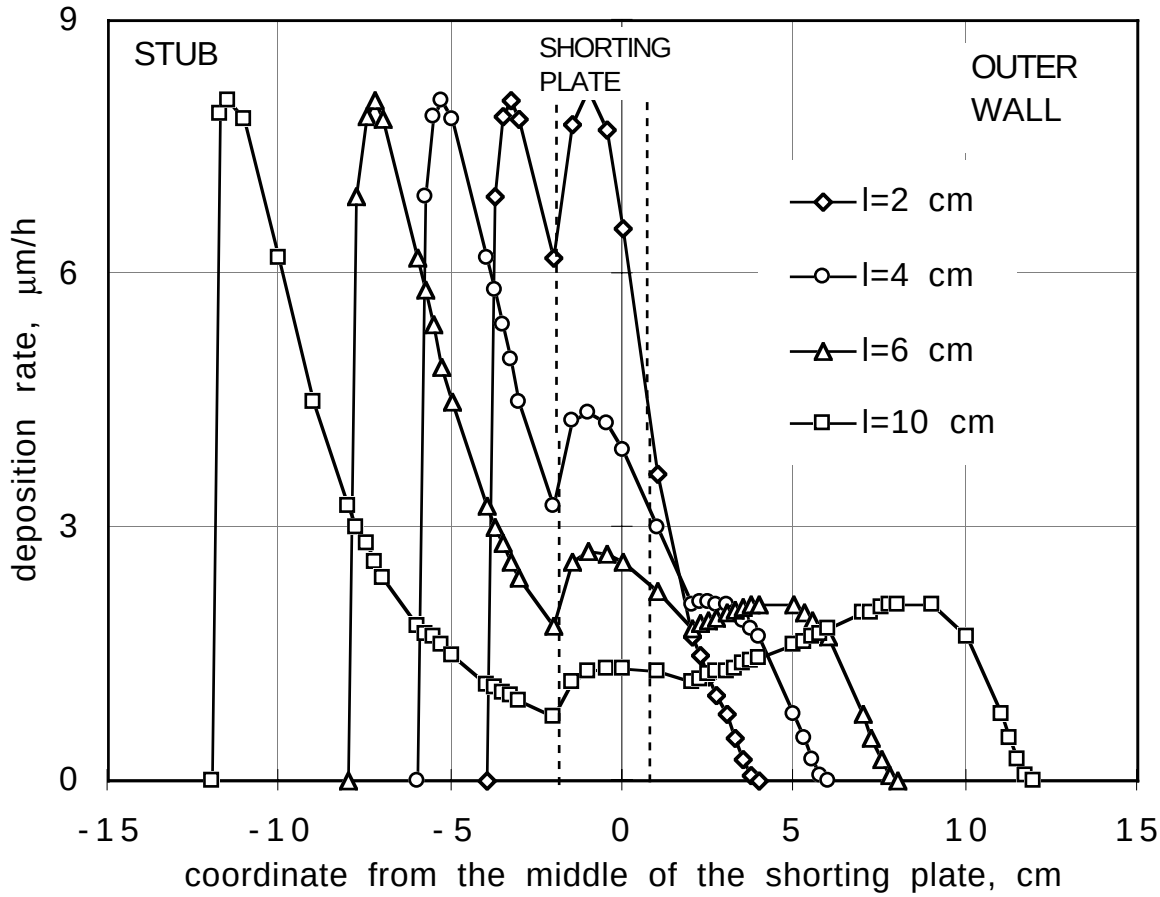

Figure 8 Calculated distribution of the deposition rate from ring cathode in Ar onto the shorting plate and onto the outer wall/stub. J = 1 A; V = 335 V.

resonator, middle of taper and the bottom as 4, 3 and 2 cm respectively. These deposition rates at 1 Amp produce less favorable conditions for the deposition of superconducting Nb film. For instance, although the maximum deposition rate exceeds the critical value of 1.5 μm/h, the average rate is about 1.1 μm/h. In the tails of distribution, with $\delta < 0.2$ μm/h, the probability of oxygen poisoning increases dramatically. Up to 50% of the film consists of niobium deposited with the rate δ <1.5 μm/h. After several scanning strokes a 'sandwich' of high RRR and low RRR layers is produced resulting in higher value of surface resistance of the film compared to the theoretical figure for pure niobium. All cathodes are not used simultaneously which produces additional 'sandwich' effects on the border layers sputtered from different cathodes.

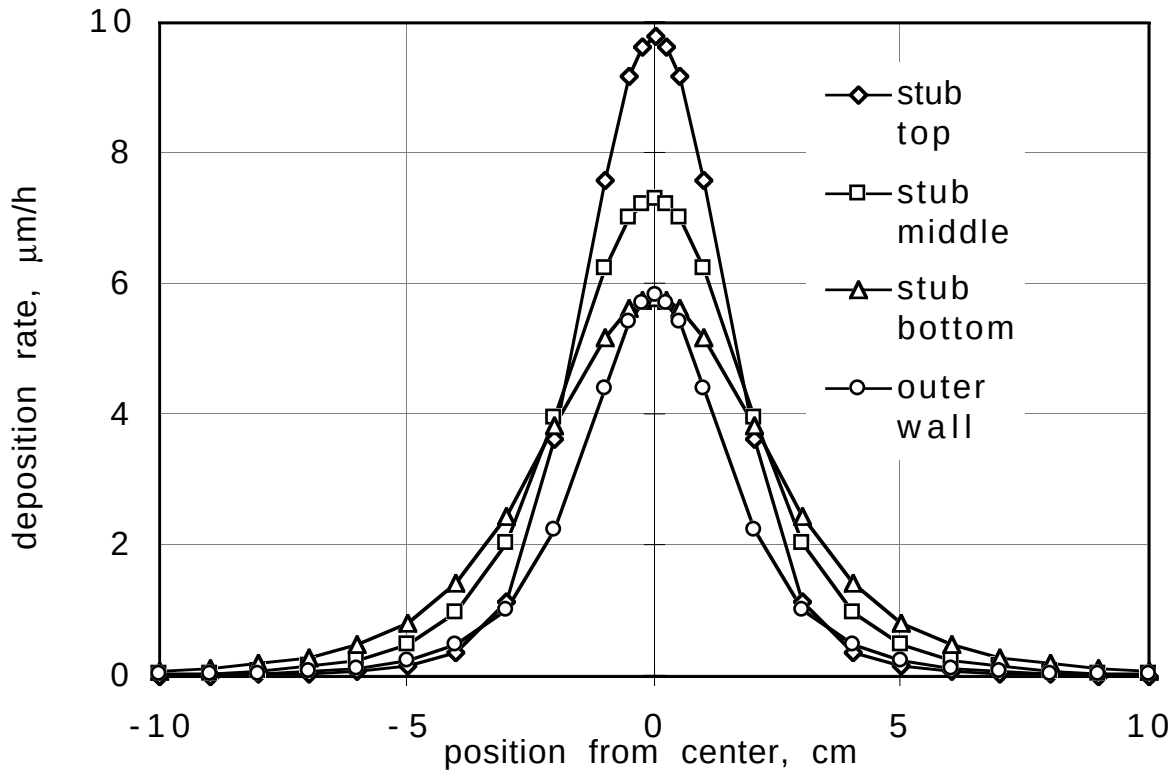

Figure 9 Calculated distribution of the deposition rate from cylindrical Nb cathode in Ar onto the outer wall/stub. J = 1 A; V = 320 V.

The quality of the Nb film can be significantly improved by simply raising the discharge current from 1 Amp up to 3 Amp which will increase the content of high RRR Nb in the film to 90% as well as allow sputtering time to be reduced to one scan thus reducing 'sandwich' effect.

Of greater importance, is to deposit Nb from the ring cathode onto the resonator walls and shorting plate in one final scan by moving it from its bottom to top position (from 20 cm below shorting plate up to 4-5 cm). In this case the low RRR Nb film will be covered by high RRR film deposited onto shorting plate in the top position of the ring cathode.

4.4 Sputtering onto Tuner Plate

The ring cathode is used also to sputter Nb onto the tuner plate of the QWR. Figure 10 shows calculated profiles for the following sputtering condition

in a separate setup: discharge current 1.0 A, discharge voltage 335 V and distance from cathode to the plate from 2, 4 and 6 cm. From this figure one

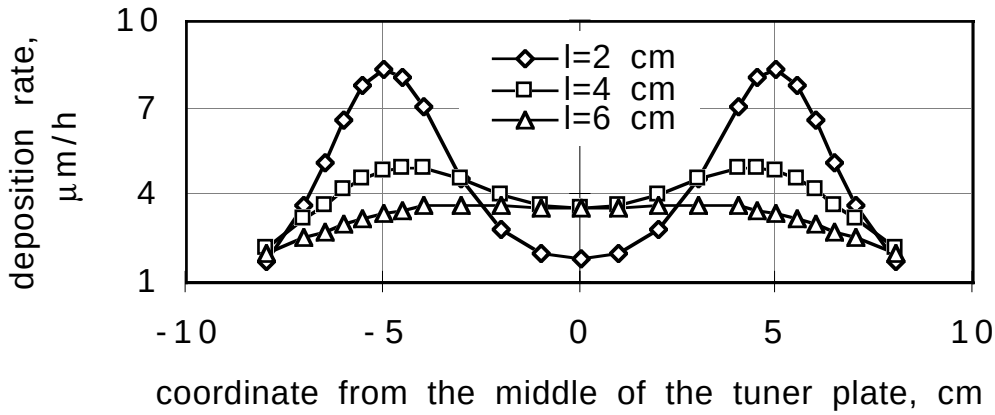

Figure 10 Calculated distribution of the deposition rate from ring cathode in Ar onto the outer tuner plate. J = 1 A; V = 335 V.

concludes that the distance of 4-5 cm provides a reasonably uniform thickness of the deposited film. In practice, Nb is sputtered onto tuner plate at 2 A for 20 min.

4.5 Nb Film Profile

During the deposition of the film, one desires a uniform coverage of resonator structures like doughnuts, beam holes, coupler and sniffer holes. To provide uniform film thickness along the resonator, the cathode assembly is scanned along the axis for a full stroke of 200 mm in 53 minutes. The film thickness profile was calculated by numerical integration of the deposition rate distribution curves (Figures 8 and 9) applied to the various surface areas of the QWR. Figure 11 shows calculated film thickness profile (thick solid line) along the resonator wall (coordinate from 0 to 61.5 cm), shorting plate (from 61.5 cm to 65.5 cm) and central electrode (from 65.5 cm to 123 cm). The discharge current for each cathode shown in Figure 11 was optimize in order to provide uniform film thickness. This requires independent operation of each side of each cylindrical cathode.

The second tool of optimization is choosing the deposition overlap between neighboring cathodes. Uniform transition from one layer of Nb to another can be achieved if the extreme positions of the middle of each cylindrical cathode are coincident. However from Figure 11, we notice the thickness is

not uniform for regions that are coated using the ring cathode. This is due the ring cathode depositing much less onto the outer wall than stub. This is not particularly surprising since it is just 0.25 cm away from stub and almost 1.1 cm from the outer wall. This smaller than optimal mean diameter is forced by the need to clear the beam hole electrodes.

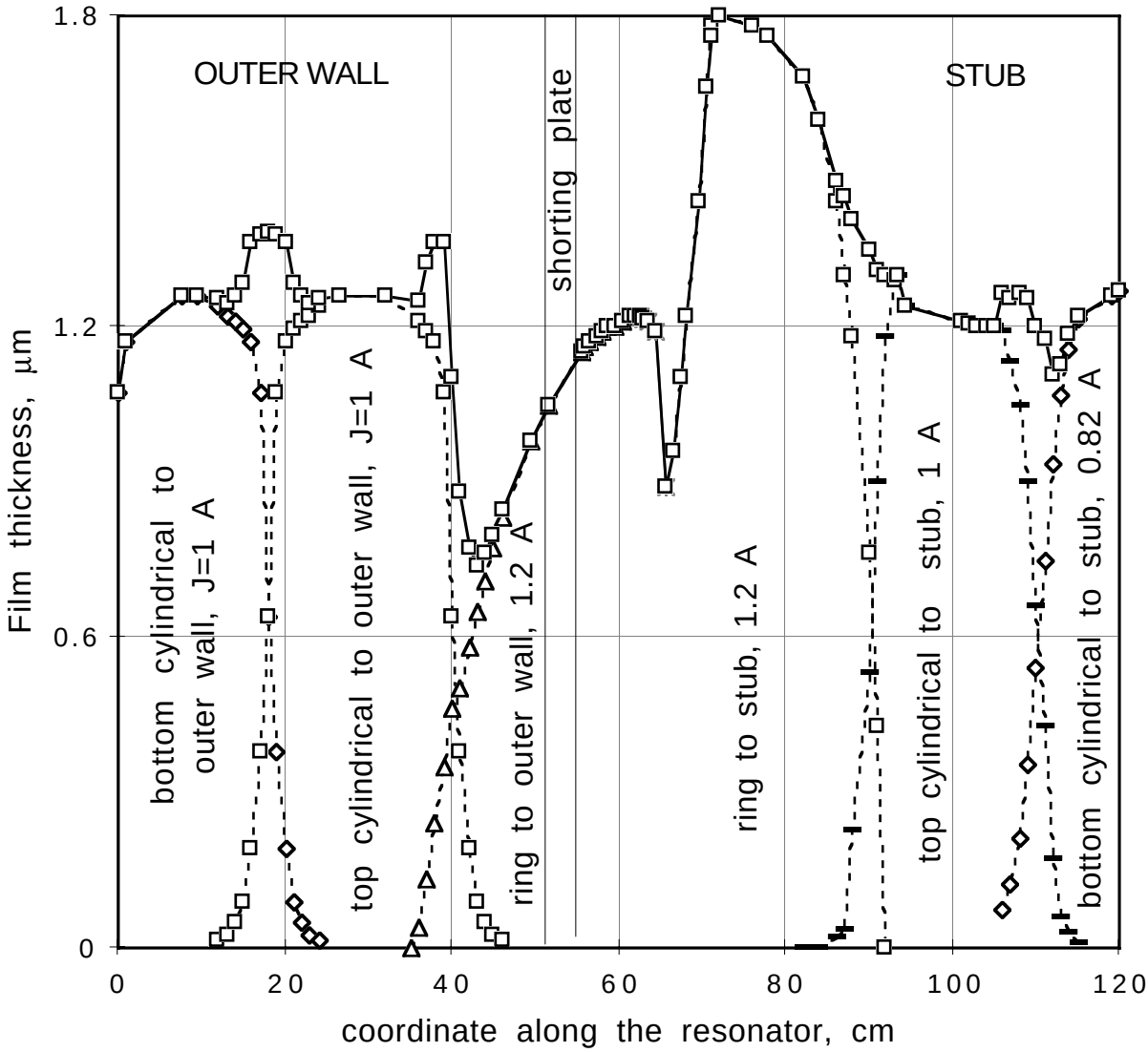

Figure 11 Deposition profiles for different cathodes (dashed lines) and resulting film thickness along the QWR (solid line).

Table 2 summarizes the sputtering/He cleaning procedure finally adopted (parameters related to cleaning in He discharge are given in bold italic).

Table 2

ANU sputtering/cleaning procedure

Cathode	Coating area	Pres mTorr	Current A	Voltage V	Coating time min	Scan range*) mm	Ext B field **)
Bot cyl	wall	3 ***50***	2.5 ***0.04***	320 ***380***	50.7 ***63***	640-450 ***640-405***	Off
Top cyl	wall	3 ***50***	2.5 ***0.04***	320 ***380***	62.7 ***63***	450-215 ***450-215***	Off
Bot cyl	stub	4	2.05	350	50.7 ***63***	640-450 ***640-405***	On
Top cyl	stub	4	2.5	350	62.7 ***63***	450-215 ***450-215***	On
Ring cath	Short stub, wall	2 ***30***	3.0 ***0.045***	335 ***300***	58 ***63***	260-40 ***260-25***	Off

*) distance from shorting plate to the middle of the erosion area;

**) external solenoid is used to switch the discharge from outer gap to inner gap in cylindrical cathodes (see section 5).

5. Plasma-surface interaction, resonator bias and the switching of the sputtering from external to internal regions.

5.1 Plasma-surface Interaction

It is generally recognized that ion bombardment during the growth of thin films produces changes in the nucleation characteristics, morphology, composition, crystalline structure, and film stress. The changes are usually attributed to resputtering of the condensing species, or to increasing the atom mobility, leading to modified microstructure of films. These characteristics are also dependent on substrate temperature. In the case of ion bombardment during film growth, it has been demonstrated that low-energy ion irradiation has an important role in controlling nucleation and growth kinetics. Bias DC sputtering has proved valuable is the deposition of superconducting Nb film for QWRs [21].

5.2 Resonator Bias

We have investigated whether the bias technique might be used also in the ANU magnetron sputtering device. The I-V characteristic of the resonator bias when the ring cathode is operated at -355 V; 1.2 A; 1.2 mTorr argon pressure is shown in Figure 12.

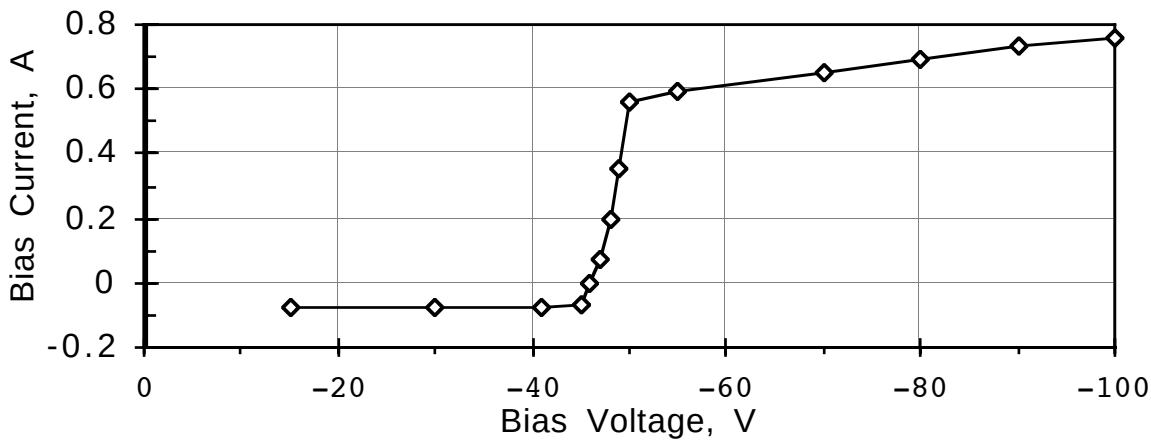

Figure 12 I-V resonator bias characteristics during cathode operation

The current collected by the resonator is shown as a function of resonator bias. In the ion saturation region of the curve, from -100 V to -50 V, the electrons are repelled and only ions are collected. When the resonator collects equal numbers of ions and electrons, the potential is equivalent to that when the resonator is insulated, i.e. the floating potential. This is about -45 V. Bias between 0 and -45 V results in negative current on the resonator.

Even with the resonator grounded, the substrate is bombarded by electrons since it is the anode. The maximum electron current flowing to a large resonator-substrate is the total discharge current. For most DC magnetrons, the ion fluxes are typically 5%-10% of the deposition flux.
Magnetron the discharge is confined in the magnetic tunnel bounded by the cathode surface and the last field line which just cuts the resonator-anode surface. The electrons move from near the cathode to this field line by collisions and are then collected by the anode. Depending on the configuration of the magnetic field, the electron/ion flux and the Nb atom flux might be separated on the resonator surface. So simultaneous deposition and bombardment might not occur in a magnetron device that employs a remote electrode to produce the bias effect.

5.3 Switching the Discharge Region

Each magnetron cathode has an individual power lead permitting independent ignition of a discharge. However the gaps on the outer and inner side of the same cylindrical cathode are intrinsically electrically in parallel. In the older cathodes, the ignition potential of the outer gap was lower than that of the inner gap and so the discharge usually existed in the outer gap only. A small magnetic field, from an external solenoid, was used to create additional leakage from the outer gap electron trap increasing its ignition potential to above the inner gap potential. Switching this solenoid controls on which side of the cylindrical cathode the discharge occurs.

The magnetic field distribution calculated using Superfish code (subroutine Pandira) with external solenoid 'Off' and 'On' is shown on Figure 13. It can be shown that the magnetic field from the external solenoid increases the integrated flux, $B_{\perp}$, over outer wall of the resonator. This destroys the electron trap resulting in higher discharge threshold voltage in outer gap. For example, during operation of the external solenoid at 3000 Amper-turns, the magnetic flux through the outer wall of the resonator increased by 58% while the magnetic flux through inner stub reduced by 13% (see Figure 13).

A very interesting option for switching the discharge was discovered using the resonator bias. When the resonator was at floating potential, the discharge existed in outer gap at working pressure below 2 mTorr. By increasing argon pressure above 2 mTorr, the internal gap discharge is

favored over the outer gap and thus controls which one is active. The water-cooled copper bases of the cylindrical cathodes were used as the anode during this test. The explanation of pressure-related discharge switch with floating resonator is still unclear.

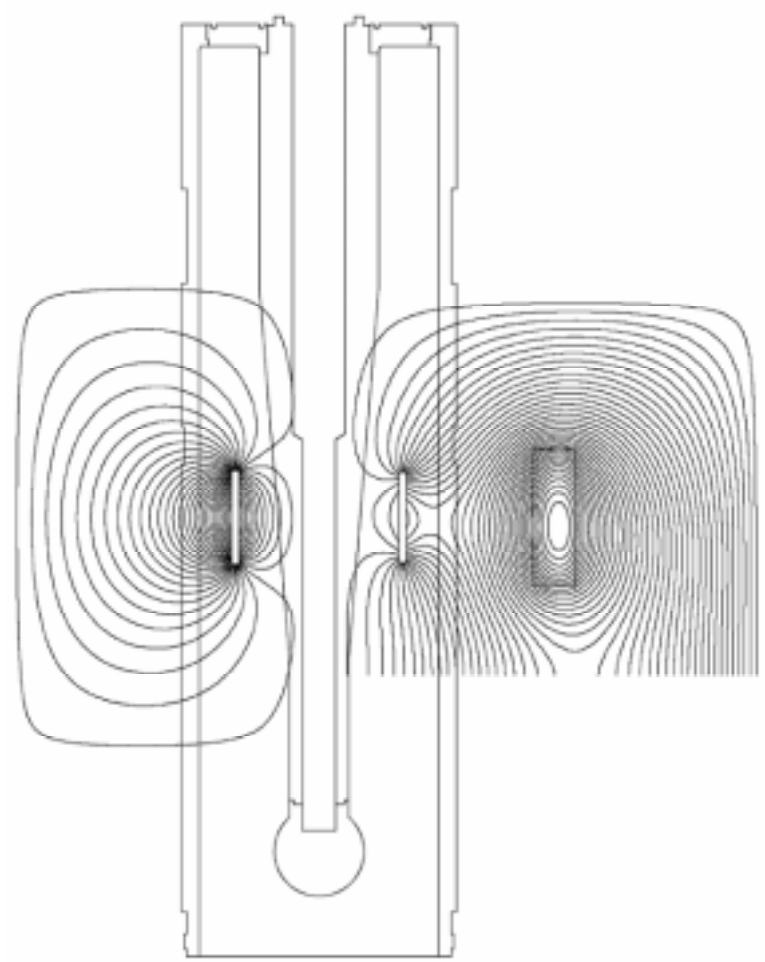

Figure 13 Superfish simulation of magnetic field distribution for cylindrical cathode with external solenoid OFF (left) and ON (right). Field ON quenches discharge between the cathode and wall allowing the cathode to stub discharge to operate. Field OFF restricts discharge to cathode to wall region.

6. Sputtering on ceramic samples and QWR. Sources of contamination of the Nb film and discussion of the ANU results

The first QWR, resonator #2, was produced in 1992 and tested in October 1993. The accelerating gradient was 1.8 MV/m, at 6 W absorbed RF power.

This resonator exhibited a disappointingly rapid drop in Q with increasing field. Although its performance is adequate for a buncher at low fields, it is not satisfactory for use in an accelerating module. Several approaches have been taken in 1994-1997 to achieve higher performance levels. These include:

- high pressure ultrapure water rinsing after chemical polishing;
- He discharge cleaning of the cathode and resonator prior to sputtering;
- sputtering at elevated substrate temperature;
- implementation of all-stainless steel feed gas system and 99.999% ultra high purity argon or helium;
- investigation of copper substrate treatments on the properties of the niobium coating

6.1 Ceramic Samples

Test sputtering on ceramic samples was the subject of extensive research. The Residual Resistivity Ratio (RRR) values, and adhesion of the Nb film were measured in order to optimize coating conditions as well the magnetron geometry. Adhesion of the niobium film is tested using a scotch tape pull away technique as well with high pressure rinsing. The quality of the Nb film is reflected in the RRR value which is related to the interstitial impurity content. The RRR was measured by the resistive method with a probable error ± 4%. Fifteen depositions were performed onto a real resonator, equipped with three ceramic samples, in order to understand the correlation between sputtering discharge parameters and superconducting properties of the coating. Depositions were carried out at a 2 - 4 mTorr argon pressure with typical power densities of 1.2 - 1.8 W/cm^2. Niobium films, 1.5 - 2 μm thick, were deposited at a current density 40 A/cm^2. It is assumed that measured RRR values are not dependent on film thickness, though ref.22 observed that the RRR values quickly decrease with decreasing Nb film thickness below 1.5 μm.

During test depositions, the bottom cylindrical cathode was kept stationary opposite the center of the sample for 40-45 min. In some tests, He discharge cleaning of the wall was performed by scanning the cathode assembly along the entire length of the resonator. During the scan, the outer wall surface is exposed to the discharge bombardment for ~600 s. The results of this series

of tests are summarized in Table 3. In all experiments, the ceramic sample in the coupler hole was sputter-coated by the ring cathode. Other samples were placed in the beam holes and coated by the lower cylindrical cathode. Because these samples were in holes, the Nb rate would be lower than on the wall and the RRR therefore lower. In Table 3, the symbol Ar refers to sputtering in Ar; He to cleaning in He discharge prior the sputtering; S to scanning the cathode; T the resonator at elevated temperature (~200°C); $Nb_{RRR=14}$ and $Nb_{RRR=142}$ to the purity of different niobium cathodes; HPR to high pressure rinsing during the resonator preparation; Ar_5 to sputtering with 5 grade (99.999% Ar) of sputtering/cleaning gas and SS to sputtering with all-stainless steel feed gas system. P_o is the base pressure.

Table 3 Experimental results of sputtering on ceramic samples

		Beam Hole		Coupl Hole		
N	Sputtering Conditions	RRR	α_b%	RRR	α_c%	P_o $x10^{-9}$ Torr
1	$Nb_{RRR=14}$, Ar	6.7	0.42	5.0	0.53	10.0
2	$Nb_{RRR=14}$,He, Ar	8.8	0.33	4.0	0.64	7.0
3	$Nb_{RRR=14}$,T,He,Ar	8.1	0.35	7.6	0.37	4.0
4	SS,HPR,$Nb_{RRR=142}$,$Ar_{5.0}$	9.2	0.31	6.5	0.43	15.0
5	SS,HPR,$Nb_{RRR=142}$,$He_{5.0}$,$Ar_{5.0}$ crack in shorting plate	10.9	0.27	6.8	0.47	10.0
6	SS,HPR,$Nb_{RRR=142}$,$He_{5.0}$,$Ar_{5.0}$ no crack in shorting plate	10.9	0.27	7.9	0.36	12.0
7	SS,HPR,$Nb_{RRR=142}$,$He_{5.0}$,$Ar_{5.0}$ resonator bias	9.7	0.3	5.5	0.49	9.0

These data may be interpreted in terms of sources of contamination during deposition. Sources of film contamination include leaks in the gas supply line, impurities in sputtering and cleaning gases and electron/photon stimulated desorption (ESD, PSD) from the resonator walls. Residual gas adsorption and outgassing are the processes controlling the ultimate pressure and gas composition before and during deposition. The mechanisms responsible for outgassing are diverse: (1) thermal desorption, (2) electron bombardment induced desorption, (3) vaporization of materials during sputtering, (4) gas diffusion from bulk and subsequent desorption [23]. Thus,

the achievement of very low partial pressures of poisonous gases is a surface-related process rather than a problem of evacuating molecules from the gas phase. In this respect, it should be mentioned that at a total pressure of 10^{-6} Torr, there are about 10^6 molecules adhering to the walls of the resonator for each molecule in the gas phase. The desorption induced by electron and photon stimulated desorption of adsorbed gases, is a problem in all sputtering systems.

Tests N = 1 to 3 were conducted with the cathode cladding made of RRR = 14 (α = 0.21%) Nb. The concentration of impurities α in Nb was calculated using formula α=3.2/(RRR-1) [3,4]. These result demonstrate a lower value of the RRR in the deposited films 4 to 9, compared to that in the sheet niobium cathode, 14. This corresponds to an introduced impurities concentration of 0.33-0.64 at.%. The best result was achieved using helium cleaning and the substrate at elevated temperature (test 3). About 40-45% reduction of RRR was observed on all samples compare to that in bulk Nb RRR=14.

Tests 4 to 7 were done with the new magnetron cathode cladding made of ultra pure Nb sheet with RRR = 142 (α=0.022%) supplied by Heraeus. Comparison of test 4 with test 1, shows that the nonstainless steel gas supply system contributed about $\alpha_{gs} \cong 0.1\%$. The tests 5 and 6 demonstrate that the crack on the shorting plate near the coupler hole introduced $\alpha_{crack} \cong 0.11\%$. The magnetron bias technique has worsened RRR (test 6 and 7) in the coupler hole. This degradation is probably caused by contamination from bias-induced-bombardment of uncoated copper surfaces.

6.2 Sources of Contamination of the Nb Film

A model describing quantitative mechanisms of desorption caused by the sputtering discharge opens a way to reduce the oxygen contamination of the Nb film [3]. In the ANU sputtering system, more than 90% of poisoning gases impinge directly on the growing film rather than being pumped away because of the high gettering pumping speed of the Nb film compared to the effective system pumping speed. The surface of the growing Nb film maintains a constant gettering speed except during a short critical period immediately after discharge ignition when little fresh Nb is present. However, during this time, plasma electron bombardment is outgassing the substrate. Under normal ANU sputtering conditions, the critical time is about 1 - 2 seconds. The critical time can be extended enhancing surface cleaning, by reducing

the deposition rate without reducing the total bombardment, the exact opposite of the goal during clean film deposition. The first step is to change the discharge atmosphere from Ar to He because the sputtering yield of Nb in He discharge is only 5-6% of that in Ar. The second is to reduce the current density during the extended cleaning phase which reduces the effective gettering speed of fresh Nb film growing during cleaning.

These preliminary data also show that higher RRR values may be obtained with elevated resonator temperature and with He cleaning discharge (tests 5 and 6). On the other hand, the results show that the RRR value of the sputtered film is still about 14 times smaller than that of the cathode material. Although, the sputtered film may never reach the purity of the cathode, it is a worthy goal. Further studies are needed to confirm this trend and define the optimum coating parameters.

7. CONCLUSION

Good quality niobium coatings with RRR values up to 11 have been produced by means of cylindrical magnetron sputtering inside QWRs. The three different cathodes are equivalent in terms of discharge characteristics and of film quality. More work is needed to define the optimum coating conditions. The QWR for the Time-Energy Lens was coated in July 1997.

Acknowledgments

We would like to express our gratitude to M.Malev for fruitful discussion, A.Rawlinson for technical assistance during sputtering. A.Muirhead carried out the precision work connected with the design and assembling of the magnetron cathode. The excellent graphic support from G.Gilmour is gratefully acknowledged.

References

[1] W. Weingarten, Non Quadratic Loss in Superconducting Sputtered Cavities for LEP, CERN-AT/93-15 (RF).

[2] M.Malev and D.C.Weisser, Nucl.Instr. and Meth. A 364 (1995) 409.

[3] M.Malev, Nucl. Instr. and Meth. A382 (1996) p.161.

[4] M. Horman, The Production of High Thermal Conductivity Niobium on a Technical Scale, Heraeus GmbH (internal report).
[5] A.Lipski,J.Noe,C.Realmuto, An Environment-Freindly Method for Resonator Surface Fabrication, SNEAP-30 to be published)
[6] J.D.Adam, et.al., CERN-85/SB/AC/B/3199/gp November 1985.
[7] P. Kneisel, B.Lewis and L.Turlington, Proc.6th Workshop on RF-Superconductivity, CEBAF (1993) p.628.
[8] H. Leidheiser, The corrosion of Copper, Tin and their alloys. R.E.Krieger Publ.Company, N.Y. 1979.
[9] F.H.P.M.Habraken and G.Bootsma, Surface Science. 97 (1980), 264-282.
[10] J.Arlow and D.Woodruff, Surface Science 157 (1985), 327-338.
[11] J.a.Thornton, J.Vac.Sci.Technol. 15/2 (1978), 171-177.
[12] J.A.Thornton and A.S.Penfold, 'Cylindrical Magnetron Sputtering in Thin Film Processes', J.L.Vossen and W.Kern, Academic Press (1978) p.75
[13] S.Rossnagel, J.Vac.Sci.Technol. A6(1), (1988) 19-24
[14] R.Frerichs,C.Kircher, J.Appl.Sci., 34/12 (1963) 3541
[15] M.Malev and D.Weisser, Nucl.Instr.Meth.Phys.Res., A364 (1995) p.409
[16] T.Motohiro J.Vac.Sci.Technol.A4(2),(1986) 189-195.
[17] W.Westwood, J.Vac.Sci.Techno. 15, 1, (1978) 1
[18] R.Somekh, J.Vac.Sci.Technol.A2(3), (1984) 1285-1291
[19] J.Sundgren in Diamond-Like Films and Coatings, ed.by R.Clausing, N.Y.(1991) 47-71.
[20] M.Malev, D.Weisser, Proc.6th Workshop on RF Superconductivity, CEBAF(1993) p.542-545.
[21] V. Palmieri et al.Proc.6th Workshop on RF Superconductivity, vol.2, 1993, pp.868-885.
[22] G.Orlandi et al., Proc.6th Workshop on RF-Superconductivity, CEBAF(1993) p.718-723.
[23] J.L.de Segovia, Vacuum 47/4 (1996), 333-340.